Multiple Weak Deflections in Galaxy-Galaxy Lensing

Tereasa G. Brainerd

Boston University, Institute for Astrophysical Research, 725 Commonwealth Ave., Boston, MA 02215

`brainerd@bu.edu`

ABSTRACT

The frequency and effects of multiple weak deflections in galaxy-galaxy lensing are investigated via Monte Carlo simulations. The lenses in the simulations are galaxies with known redshifts and known rest-frame blue luminosities. The frequency of multiple deflections above a given threshold shear value is quantified for discrete source redshifts, as well as for a set of sources that are broadly distributed in redshift space. In general, the closest lens in projection on the sky is not the only lens for a given source. In addition, $\sim 50\%$ of the time the closest lens is not the most important lens for a given source. Compared to a naive single-deflection calculation in which only the lensing due to the closest weak lens is considered, a full multiple-deflection calculation yields a higher net shear for individual sources, as well as a higher mean tangential shear around the lens centers. The full multiple-deflection calculation also shows that galaxy-galaxy lensing may contribute a substantial amount to cosmic shear on small angular scales. The degree to which galaxy-galaxy lensing contributes to the small-scale cosmic shear is, however, quite sensitive to the mass adopted for the halos of L_B^* galaxies. Changing the halo mass by a factor of ~ 2.5 changes the contribution of galaxy-galaxy lensing to the cosmic shear by a factor of ~ 3 on scales of $\theta \sim 1$ arcmin. The contribution of galaxy-galaxy lensing to cosmic shear decreases rapidly with angular scale and extrapolates to zero at $\theta \sim 5$ arcmin. This last result is roughly independent of the halo mass and suggests that for scales $\theta \gtrsim 5$ arcmin, cosmic shear is insensitive to the details of the gravitational potentials of large galaxies.

Subject headings: dark matter – galaxies: halos – gravitational lensing

1. Introduction

Galaxy-galaxy lensing is the systematic weak gravitational lensing of background galaxies by foreground galaxies. Unlike weak lensing by massive galaxy clusters, where the only important lens in the problem is the cluster itself, galaxy-galaxy lensing involves multiple weak deflections. For example, it is common for a distant source galaxy at redshift z_s to be weakly lensed by a more nearby galaxy at redshift z_{l1}, and for both of these galaxies to then be lensed by another (even more nearby) galaxy at redshift z_{l2}. Thus, the galaxy with redshift z_{l1} serves simultaneously as a lens for the galaxy at z_s and a source for the galaxy at z_{l2}. In addition, the galaxy at z_s is lensed by two independent foreground galaxies. The importance of such multiple deflections in galaxy-galaxy lensing was first noted by Brainerd et al. (1996; hereafter BBS). Since the work of BBS, galaxy-galaxy lensing has been detected with impressively high statistical significance by a number of different groups. This has enabled constraints to be placed on the nature of the dark matter halos that surround the lens galaxies as well as the bias between mass and light in the universe (see, e.g., Fischer et al. 2000; Guzik & Seljak 2002; Hoekstra et al. 2004, 2005; Sheldon et al. 2004; Heymans et al. 2006; Kleinheinrich et al. 2006; Mandelbaum et al. 2006ab; Limousin et al. 2007; Parker et al. 2007; Natarajan et al. 2009; Tian et al. 2009).

The purpose of the present investigation is to: (i) quantify the frequency of multiple weak lensing deflections in a relatively deep galaxy-galaxy lensing data set, (ii) determine the effect of multiple deflections on the net shear for distant source galaxies that have been weakly lensed by foreground galaxies, and (iii) demonstrate that galaxy-galaxy lensing alone may contribute a substantial amount to the "cosmic shear" signal on small angular scales. To do this, theoretical shear fields are constructed using a set of observed galaxies with known redshifts and known rest-frame blue luminosities. A simple halo model is used to assign masses to the observed galaxies and Monte Carlo simulations are then used to lens various theoretical source galaxy distributions by the observed galaxies. Theoretical shear fields for full, multiple-deflection calculations are computed; i.e., each source galaxy in the simulation is lensed by all foreground galaxies. In addition, theoretical shear fields for naive, single-deflection calculations (where the closest lens on the sky is assumed to be the only lens) are also computed. The results of the single-deflection calculations are compared to those of the full, multiple-deflection calculations in order to assess the effects of multiple deflections in galaxy-galaxy lensing. Throughout, the weak lensing of an entire source galaxy by a single foreground lens galaxy will be referred to as a "deflection".

The paper is organized as follows. The Monte Carlo simulations of galaxy-galaxy lensing are described in Section 2, the frequency of multiple weak deflections in galaxy-galaxy lensing is computed in Section 3, the effects of multiple weak deflections on the galaxy-galaxy lensing

shear are computed in Section 4, the contribution of galaxy-galaxy lensing to cosmic shear is computed in Section 5, and a discussion of cosmic variance in relation to the field size in presented in Section 6. The conclusions are summarized in Section 7.

2. Monte Carlo Simulations of Galaxy-Galaxy Lensing

To investigate the frequency and effects of multiple weak deflections in galaxy-galaxy lensing, Monte Carlo simulations are constructed. The lens galaxies in the Monte Carlo simulations are relatively bright galaxies that are contained within a circle of radius 4 arcmin, centered on the Hubble Deep Field North (HDF-N) (Williams et al. 1996). This region of sky was the subject of a deep redshift survey (Cohen et al. 1996; Steidel et al. 1996; Lowenthal et al. 1997; Phillips et al. 1997; Cohen et al. 2000) as well as an extensive multicolor photometric investigation (Hogg et al. 2000). As a result, both the redshifts (Cohen et al. 2000, Tables 2A and 2B) and rest-frame blue luminosities, L_B (Cohen 2001, Table 1), of 590 galaxies in this region of the sky are known. For the simulations, then, the locations of the lenses in redshift space are known very accurately, and the relative strengths of the different lenses can be inferred quite well from their relative luminosities. Therefore, it is possible to make detailed theoretical predictions for the weak galaxy-galaxy lensing shear field that should be expected in this region of sky.

For simplicity, the dark matter halos of the lens galaxies are taken to have a mass density given by

$$\rho(r) = \frac{\sigma_v^2 s^2}{2\pi G r^2 \left(r^2 + s^2\right)}, \tag{1}$$

where σ_v is the velocity dispersion of the halo, G is Newton's constant, and s is a characteristic halo radius (see e.g., BBS; Hudson et al. 1998; Fischer et al. 2000; Hoekstra et al. 2004). It is then convenient to scale the depths of the potential wells of lens galaxies with differing luminosities, L_B, according to a Tully-Fisher or Faber-Jackson type of relation

$$\frac{\sigma_v}{\sigma_v^*} = \left(\frac{L_B}{L_B^*}\right)^{1/4}, \tag{2}$$

where σ_v^* is the velocity dispersion of the halo of a lens galaxy with rest-frame blue luminosity L_B^*. Again for simplicity, it is assumed that the mass-to-light ratio of a galaxy is constant independent of its luminosity. Therefore, the characteristic radii of the halos of galaxies with $L_B \neq L_B^*$ scale with the radii of the halos of L_B^* galaxies as

$$\frac{s}{s^*} = \left(\frac{L_B}{L_B^*}\right)^{1/2}. \tag{3}$$

Under these assumptions, then, the mass of the halo of an L_B^* galaxy is given by

$$M^* = \frac{\pi s^* (\sigma_v^*)^2}{G} \qquad (4)$$

and the deflection of a light ray emanating from a source galaxy is given by

$$\alpha(X) = \frac{4\pi \sigma_v^2 D_{ls}}{D_s X c^2} \left[1 + X - \left(1 + X^2 \right)^{1/2} \right]. \qquad (5)$$

Here D_s is the angular diameter distance between the observer and the source, D_{ls} is the angular diameter distance between the lens and the source, and X is the ratio of the impact parameter of the light ray and the characteristic radius, s, of the lens (i.e., $X \equiv R/s$; see BBS).

It is worth noting that galaxy-galaxy lensing has, of course, been detected in the HDF-N (e.g., dell'Antonio & Tyson 1996; Hudson et al. 1998); however due to the very small number of galaxies in the HDF-N, the galaxy-galaxy lensing signal can only be detected with relatively low significance. In particular, there are simply too few actual source galaxies to carry out a detailed investigation of the effects of multiple deflections using only the observed sources. It is for this reason that Monte Carlo simulations are adopted here.

The completeness limits of the redshift survey are, unfortunately, different for the HDF-N itself and the surrounding area of the sky, the survey being deeper in the region of the HDF-N. This gives rise to a somewhat different redshift distribution for galaxies with measured redshifts in the center of the field versus galaxies with measured redshifts in the outer region of the field. In order to make an accurate prediction for the theoretical shear field, it is important that the redshift completeness limit for the lenses in the Monte Carlo simulations be uniform across the field. Therefore, a conservative completeness limit of $R = 23$ is imposed here, and the lenses in the Monte Carlo simulations consist of the 427 galaxies with $R \le 23$ in Cohen et al. (2000) and Cohen (2001) for which spectroscopic redshifts and rest-frame blue luminosities are known. The median redshift of the lens galaxies is therefore $z_{\mathrm{med}} = 0.55$.

Two approaches are taken to model the redshifts of the source galaxy population: (i) source galaxies are simply placed in a single plane of redshift z_s and (ii) source galaxies are distributed in redshift space according to the observed redshift distribution of faint galaxies. The first approach allows an investigation of the frequency of multiple weak deflections as a function of discrete source redshift. The second approach demonstrates the overall effect that would be expected to occur in a deep galaxy-galaxy lensing data set.

Each Monte Carlo simulation includes 10 million source galaxies that are assigned random positions (RA and DEC) within a circle of radius 2.5 arcminutes, centered on the HDF-N. The sources are contained within a smaller area than the lenses because, as will

be shown below, about 10% of the time the most important lens for a given source may be more than an arcminute away. By restricting the sources to a smaller area than the lenses, edge effects (in which sources are not properly lensed by all foreground galaxies) are avoided. In simulations where the sources are restricted to a single plane in redshift space, each source is assigned the identical redshift, z_s. In simulations where the sources are broadly distributed in redshift space, the apparent magnitudes of the sources are taken to be in the range $19 < I < 25$, and the number of sources per unit magnitude is chosen to match the observed number counts in the I-band (e.g., Smail et al. 1995). These sources are assumed to follow a redshift distribution of the form

$$P(z|I) = \frac{\beta z^2 \exp\left[-(z/z_0)^\beta\right]}{\Gamma(3/\beta)z_0^3}, \tag{6}$$

which is in good agreement with the redshift surveys of LeFèvre et al. (1996) and LeFèvre et al. (2004). Assuming $\beta = 1.5$ and extrapolating the results of LeFèvre et al. (2004) to a sample of galaxies with $19 < I < 25$ yields

$$z_0 = 0.8\left[0.86 + 0.15(I - 23.35)\right] \tag{7}$$

(see, e.g., BBS). The median redshift of the sources in this case is $z_{\mathrm{med}} = 0.96$.

Throughout, we will consider only the weak lensing regime. That is, we will restrict our analysis to the case that the surface mass density of the lenses is very much less than the critical surface mass density for strong lensing ($\Sigma(\theta) << \Sigma_c \equiv \frac{c^2}{4\pi G}\frac{D_s}{D_d D_{ls}}$), the deflection angle, α, the modulus of the shear, γ, and the convergence, κ, are all small, and $\gamma \simeq \kappa$. Given that the physical size of each lens is very much smaller than the distances between the observer, lens, and source, we will adopt the standard thin lens approximation (e.g., Blandford & Narayan 1986; Schneider et al. 1992). Further, we will perform all calculations in the framework of the Born approximation, in which integrations are performed along an undeflected light ray. This standard weak lensing formalism is valid even in the limit of multiple weak deflections (e.g., Bartelmann & Schneider 2001). Indeed, investigations into the degree to which the Born approximation may affect predictions of cosmic shear (where the weak lenses consist of all the mass along the line of sight), have shown that corrections due to the Born approximation are two to three orders of magnitude smaller than the cosmic shear signal itself (e.g., Cooray & Hu 2001; Hilbert et al. 2009).

For each Monte Carlo simulation, specific values of the velocity dispersion, σ_v^*, and characteristic radius, s^*, for L_B^* galaxies are chosen. Velocity dispersions, σ_v, and characteristic radii, s, are then assigned to each lens galaxy based upon the above scaling relations. The redshifts of the lenses, z_l, are taken to be the observed spectroscopic redshifts, and the positions of the lenses in the field (RA and DEC) are taken to be the observed positions on

the sky. The Monte Carlo simulation then proceeds by computing the weak lensing shear, $\vec{\gamma}$, that is induced as the light rays emanating from the background sources encounter the foreground lenses. In the case of single-deflection calculations, the lensing of each source is computed solely for the lens which is nearest to the source in projection on the sky. That is, the "closest" lenses are the only lenses that are used in the single deflection calculations, and the resulting shear for each source is simply the shear induced by the closest lens. In the case of full, multiple-deflection calculations, the lensing of each source by all foreground lenses is computed. The resulting shear for each source is then the net shear due to all foreground lenses. This is straightforward to compute in the weak lensing regime since all weak deflections may be considered to be independent (e.g., Bartelmann & Schneider 2001).

Each source galaxy is assigned a random intrinsic position angle and an intrinsic ellipticity that is drawn at random from the observed ellipticity distribution of the HDF-N galaxies. The intrinsic shape parameters of the source galaxies are then given by

$$\vec{\chi}_{in} = \epsilon_{in} \; e^{2i\phi_{in}} \tag{8}$$

where $\epsilon_{in} = (a - b)/(a + b)$ is the intrinsic ellipticity of the source and ϕ_{in} is its intrinsic position angle. Since we are dealing only with the weak lensing regime, the final image shape of each source galaxy in the multiple-deflection calculations is given by

$$\vec{\chi}_f = \vec{\chi}_{in} + \Sigma_{j=1}^{N_{\text{lens}}} \; \vec{\gamma}_j \tag{9}$$

where $\vec{\gamma}_j$ is the shear induced by foreground lens galaxy, j. In the case of the full, multiple-deflection calculations, the net shear due to all lenses with $z_l < z_s$ is used to obtain $\vec{\gamma}_f$ for each source galaxy. In the case of the single deflection calculations, the sum over all foreground lenses is simply replaced by $\vec{\gamma}_{\text{close}}$, the shear induced by the lens that is closest to the source in projection on the sky.

Shown in Figure 1 is a zoomed-in image of one of the simulations. The image is centered on the HDF-N, and the locations of chips 2, 3, and 4 on WFPC-2 are shown by the black lines. Here a fiducial lens halo model with $\sigma_v^* = 150$ km sec^{-1} and $s = 100h^{-1}$ kpc has been adopted, and the source galaxies have been distributed in redshift space according to equation (6) above. A flat Λ-dominated cosmology with $H_0 = 70$ km sec^{-1} Mpc^{-1}, $\Omega_{m0} = 0.3$ and $\Omega_{\Lambda 0} = 0.7$ has been also been adopted. The left panel of Figure 1 shows the magnitude of the net shear, and for clarity the orientation of the net shear is not shown. Red peaks in the shear field (i.e., locations of the largest net shear) correspond to the locations of the most important weak galaxy lenses in the field. The right panel of Figure 1 shows the surface mass density of the lens galaxies. Note that some very luminous (and, therefore very massive) galaxies do not show up in the shear field due to the fact that their redshifts place them well beyond the median redshift of the sources. A good example of this is the galaxy

located at $(-23.20, +56.70)$ in Figure 1. This galaxy has coordinates on the sky of RA $=$ 12^h 36^m 52.72^s, DEC $= +62°$ $13'$ $54.70''$ (J2000). Its rest-frame blue luminosity is $2.95L_B^*$ and, hence, its halo mass is $6.9 \times 10^{12} M_\odot$ (for the fiducial model). The center of this galaxy has a high surface mass density (indicated by red in the right panel of Figure 1). However, since the redshift of this galaxy is $z = 1.355$, it cannot act as a lens for the majority of the sources. Therefore, it does not contribute substantially to the net shear field. By contrast, the two smaller galaxies that are immediately to the east and west of this intrinsically very bright and massive galaxy do show up quite prominently in the shear field. These galaxies have coordinates on the sky of RA $= 12^h$ 36^m 54.07^s, DEC $= +62°$ $13'$ $54.20''$ and RA $=$ 12^h 36^m 51.77^s, DEC $= +62°$ $13'$ $53.70''$, corresponding to locations of $(-32.65, +56.20)$ and $(-16.56, +55.70)$ in Figure 1. These two galaxies have luminosities of $L_{\text{east}} = 0.70 L_B^*$ and $L_{\text{west}} = 0.87 L_B^*$, and redshifts of $z_{\text{east}} = 0.851$ and $z_{\text{west}} = 0.557$. Both of these galaxies are assigned very similar halo masses in the simulation (since their luminosities are very similar), and both are clearly visible in the shear field as red peaks. However, the easternmost of these two galaxies corresponds to a smaller peak in the shear field than the westernmost because the redshift of the easternmost galaxy is only slightly less than the median redshift of the sources, while the redshift of the westernmost galaxy is of order half the median redshift of the sources. For a color image of the HDF-N in which the redshifts of the galaxies are indicated, the reader is encouraged to see Figure 2 of Cohen et al. (2000).

3. Frequency of Multiple Deflections

The probability that a given source galaxy will have been weakly-lensed by one or more foreground galaxies is, of course, a strong function of the actual value of the shear, γ, induced by a given weak lensing deflection. That is, it is much more likely for a distant galaxy to be lensed by a foreground galaxy which produces an insignificant weak shear of $\gamma \sim 10^{-6}$ than, say, a relatively large weak shear of $\gamma \sim 0.01$. Therefore, in order to discuss the total number of weak deflections that a given source galaxy is likely to encounter, a decision has to be made as to what value of γ qualifies as a "significant" value of the shear. A typical value of the shear induced by a single weak galaxy lens is $\gamma \sim 0.005$ (see, e.g., BBS) and this value of γ will be used as a baseline for computing the number of weak lensing deflections that source galaxies have undergone in the Monte Carlo simulations.

To begin this section, the Monte Carlo simulations will be restricted to the fiducial halo lens model from the previous section in which $\sigma_v^* = 150$ km sec^{-1} and $s^* = 100 h^{-1}$ kpc, and sources will be placed in single planes in redshift (i.e., all sources will be assigned identical redshifts). Figures 2, 3, and 4, then, show the probability, $P(N_L)$, that a given source with
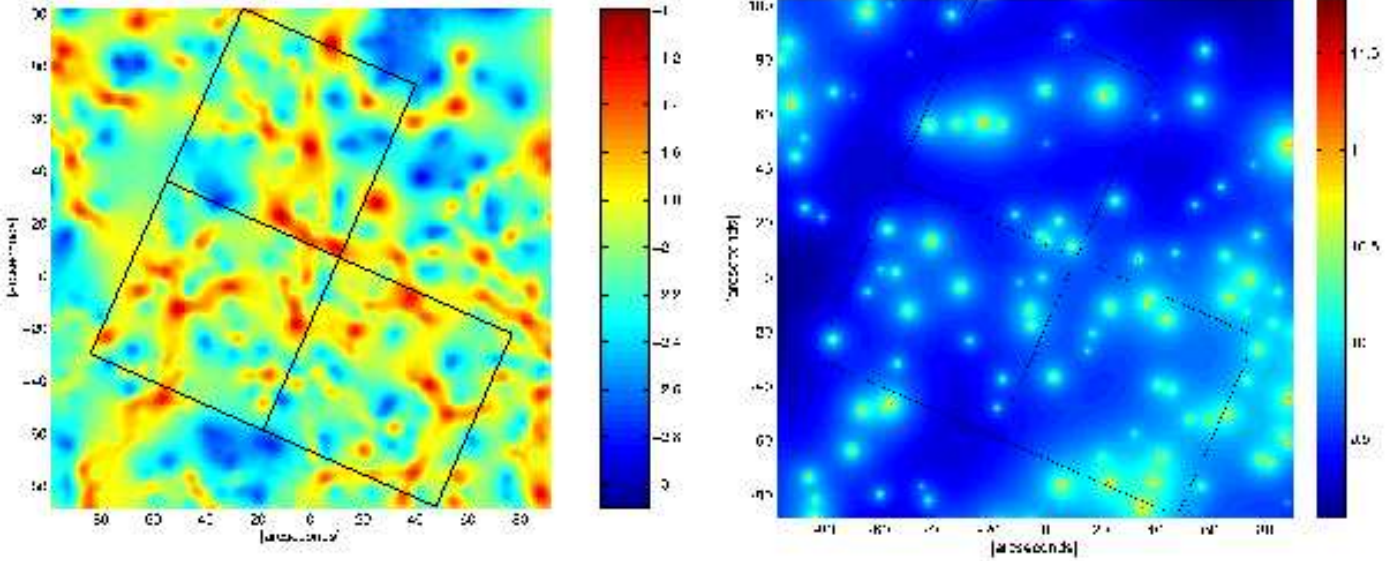
Fig. 1.— A localized region of a simulation, centered on the HDF-N. The figure has been oriented according to the standard convention (i.e., "North" is up, and "East" is to the left). The characteristic chevron of WFPC-2 is indicated by the black lines. Note that in the full simulations, the lens galaxies are contained within an area that is ~ 16.5 times larger than the HDF-N. A fiducial halo model with $\sigma_v^* = 150$ km sec^{-1} and $s^* = 100h^{-1}$ kpc, and cosmological parameters $H_0 = 70$ km sec^{-1} Mpc^{-1}, Ω_{m0}, and $\Omega_{\Lambda 0}$ have been adopted. The median redshift of the lenses is $z_l = 0.55$ and the median redshift of the sources is $z_s = 0.96$. Left: Logarithm of the net shear produced by the lens galaxies. Peaks in the shear field correspond to the most important weak galaxy lenses in the localized region of the HDF-N. Right: Logarithm of the surface mass density of the lens galaxies. Here the units of surface mass density are solar masses per square arcsecond. Due to their redshifts being much greater than the median redshift of the sources, some galaxies that contribute significantly to the surface mass density do not contribute significantly to the shear field. Conversely, some galaxies that contribute relatively little to the surface mass density contribute a substantial amount to the shear field because their redshifts are considerably smaller than the median redshift of the sources.

redshift z_s will be lensed by N_L foreground galaxies, where each *individual deflection* gives rise to a shear of $\gamma > 0.0025$, $\gamma > 0.005$, and $\gamma > 0.01$, respectively (i.e., the minimum shear in these figures corresponds to half the baseline value, the baseline value, and twice the baseline value, respectively). Here $P(N_D = 2)$ is the probability that a given source will be lensed by two individual foreground galaxies, each of which lensed the source galaxy at a level that is comparable to or greater than the minimum shear value. Since the minimum values adopted in Figures 2, 3, and 4 are "substantial" values of the galaxy-galaxy lensing shear, the results shown in these figures are conservative estimates of the frequency of multiple deflections. The line types in Figures 2, 3, and 4 correspond to different values of the cosmological parameters. In all cases $H_0 = 70$ km sec^{-1} Mpc^{-1} is adopted. Solid lines show results for a flat Λ-dominated universe with $\Omega_{m0} = 0.3$ and $\Omega_{\Lambda 0} = 0.7$, dashed lines show results for an open universe with $\Omega_{m0} = 0.3$ and $\Omega_{\Lambda 0} = 0.0$, and dotted lines show results for an Einstein-de Sitter universe.

Figures 2, 3, and 4 demonstrate two fully expected results. First, the frequency of multiple deflections in galaxy-galaxy lensing is a function of the source redshift: the higher the redshift, the more likely multiple deflections are to occur. Second, the frequency of multiple deflections in galaxy-galaxy lensing depends upon the minimum shear value that is adopted: the lower the value of the minimum shear, the more likely that multiple deflections of at least the minimum value will occur. Figure 2 shows that multiple deflections in which each individual deflection results in a shear of $\gamma > 0.0025$ are highly probable. The probability ranges from 67% for sources with $z_s = 0.75$ to 100% for sources with $z_s = 2.0$. Similarly, Figure 3 shows that multiple deflections in which each individual deflection results in a shear of $\gamma > 0.005$ are highly probable. In this case, the probability ranges from 23% for sources with $z_s = 0.75$ to 92% for sources with $z_s = 2.0$. Multiple deflections in which each individual deflection results in a shear of $\gamma > 0.01$ are relatively rare for sources with $z_s \leq 1.0$, but the probability of such very large multiple deflections increases to 45% for sources with $z_s = 2.0$ (Figure 4).

In addition to the frequency of multiple deflections, Figures 2, 3, and 4 make an important point about the role of the cosmological parameters in galaxy-galaxy lensing. By and large, the number and magnitude of individual weak lensing deflections is unaffected by the choice of the cosmological parameters. That is, galaxy-galaxy lensing primarily provides information about the potentials of the lens galaxies, not the cosmology per se (see also BBS). Therefore, for the remainder of the manuscript a flat Λ-dominated universe with $H_0 = 70$ km sec^{-1} Mpc^{-1}, $\Omega_{m0} = 0.3$, and $\Omega_{\Lambda 0} = 0.7$ will be adopted.

While galaxy-galaxy lensing is largely insensitive to the values of the cosmological parameters, it is quite sensitive to masses of the halos of the lens galaxies. The dependence of
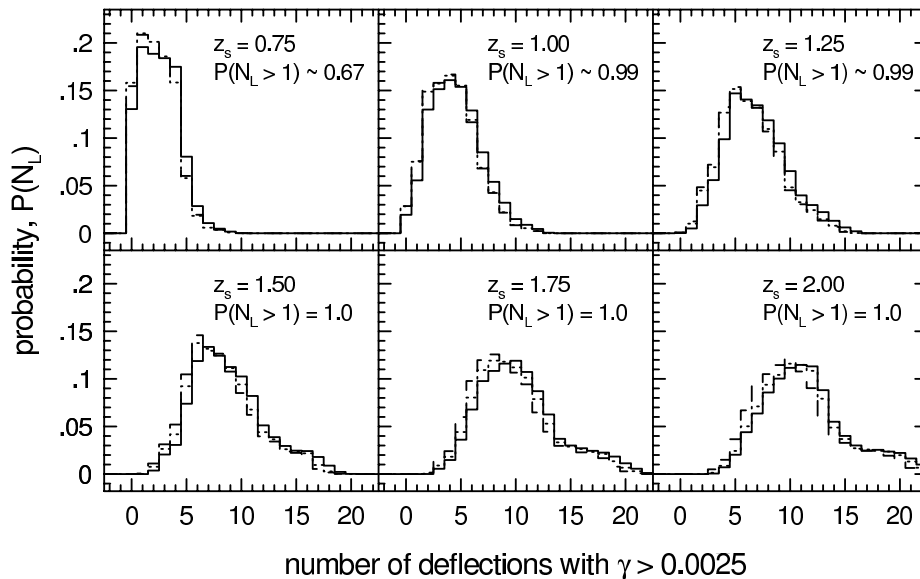
Fig. 2.— Probability, $P(N_L)$, that a source galaxy with redshift z_s will be lensed by N_L foreground galaxies, where each individual lens induces a shear $\gamma > 0.0025$. For $N_L > 1$, multiple deflections with $\gamma > 0.0025$ have been experienced by the source. Source redshifts range from $z_s = 0.75$ (top left) to $z_s = 2.0$ (bottom right). The median lens redshift is $z_l = 0.55$. A fiducial halo model with $\sigma_v^* = 150$ km sec^{-1} and $s^* = 100h^{-1}$ kpc has been adopted. Line types correspond to different values of the cosmological parameters. Solid lines: flat Λ-dominated universe. Dashed lines: open universe. Dotted lines: Einstein-de Sitter universe.
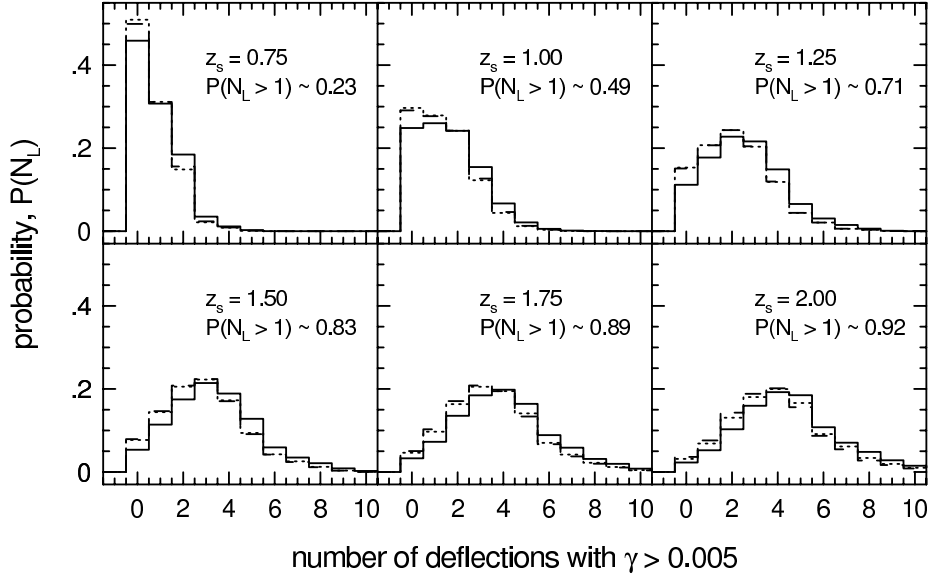
Fig. 3.— Same as Figure 2, except here the frequency of deflections with $\gamma > 0.005$ is shown. For $N_L > 1$, multiple deflections have been experienced by the source.
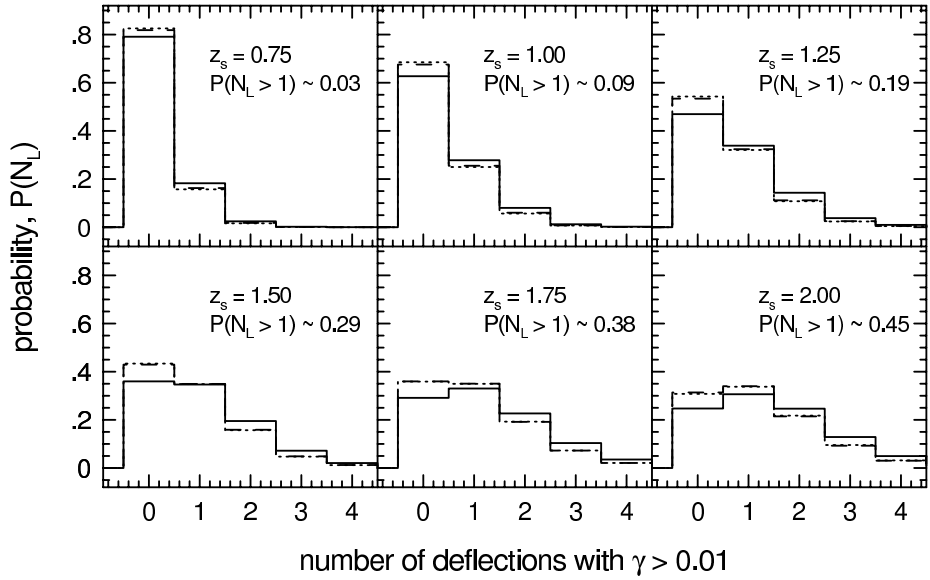

Fig. 4.— Same as Figure 2, except here the frequency of deflections with $\gamma > 0.01$ is shown. For $N_L > 1$, multiple deflections have been experienced by the source.

galaxy-galaxy lensing on the physical radii of the halos of the lens galaxies is rather weak (see, e.g., BBS; Hoekstra et al. 2004; Kleinheinrich et al. 2006); however, the dependence of galaxy-galaxy lensing on the velocity dispersions of the halos of the lens galaxies is quite strong. The effect of varying the characteristic lens parameters on the frequency of multiple weak deflections is shown in Figures 5, 6, and 7. In contrast with Figures 2, 3, and 4, here the source galaxies have been distributed broadly in redshift space (as in Figure 1), with a median source redshift of $z_s \sim 0.96$. The characteristic halo parameters for L_B^* galaxies are varied as follows: $\sigma_v^* = 135$ km sec^{-1}, $\sigma_v^* = 150$ km sec^{-1}, $\sigma_v^* = 165$ km sec^{-1}; $s^* = 50h^{-1}$ kpc, $s^* = 100h^{-1}$ kpc, $s^* = 200h^{-1}$ kpc. As in Figures 2, 3, and 4, the shear produced by each individual deflection is restricted to $\gamma > 0.0025$ (Figure 5), $\gamma > 0.005$ (Figure 6), and $\gamma > 0.01$ (Figure 7).

For the adopted source redshift distribution, then, the probability of multiple weak deflections increases as the characteristic mass of the halos of L_B^* lens galaxies increases. That is, the larger is the mass of the lens, the wider is its aperture of influence on the sky. For the adopted source redshift distribution, there is a high probability of multiple deflections in which each individual deflection results in a shear of $\gamma > 0.0025$. The probability ranges from 54% for the lowest characteristic halo mass (Figure 5, top left) to 82% for the highest characteristic halo mass (Figure 5, bottom right). Similarly, there is a high probability of multiple deflections in which each individual deflection results in a shear of $\gamma > 0.005$. The probability ranges from 26% for the lowest characteristic halo mass (Figure 6, top left) to 59% for the highest characteristic halo mass (Figure 6, bottom right). From Figure 7, instances of multiple deflections in which each individual deflection results in a very substantial shear of $\gamma > 0.01$ are relatively rare for low values of σ_v^* and s^*. However, for large values of σ_v^* and s^*, the probability can exceed 20%. Note that, at fixed impact parameter, the deflection angle, α, caused by L_B^* lenses scales as essentially $s^*(\sigma_v^*)^2$. So, for a lens with a given velocity dispersion, the deflection angle scales approximately linearly with s^*. This naturally leads to larger induced shear for larger values of s^*, and a correspondingly larger number of individual deflections that exceed the minimum shear thresholds used in Figures 5-7.

4. Multiple Deflections vs. Single Deflections

The previous section explored the frequency with which source galaxies undergo multiple weak deflections in a deep galaxy-galaxy lensing data set. This section will explore how the net shear, γ_{net}, obtained from a full, multiple-deflection calculation compares to the shear obtained solely from the closest lens in projection on the sky (γ_{close}), as well as how the net shear compares to the shear resulting from the largest individual deflection in the multiple-
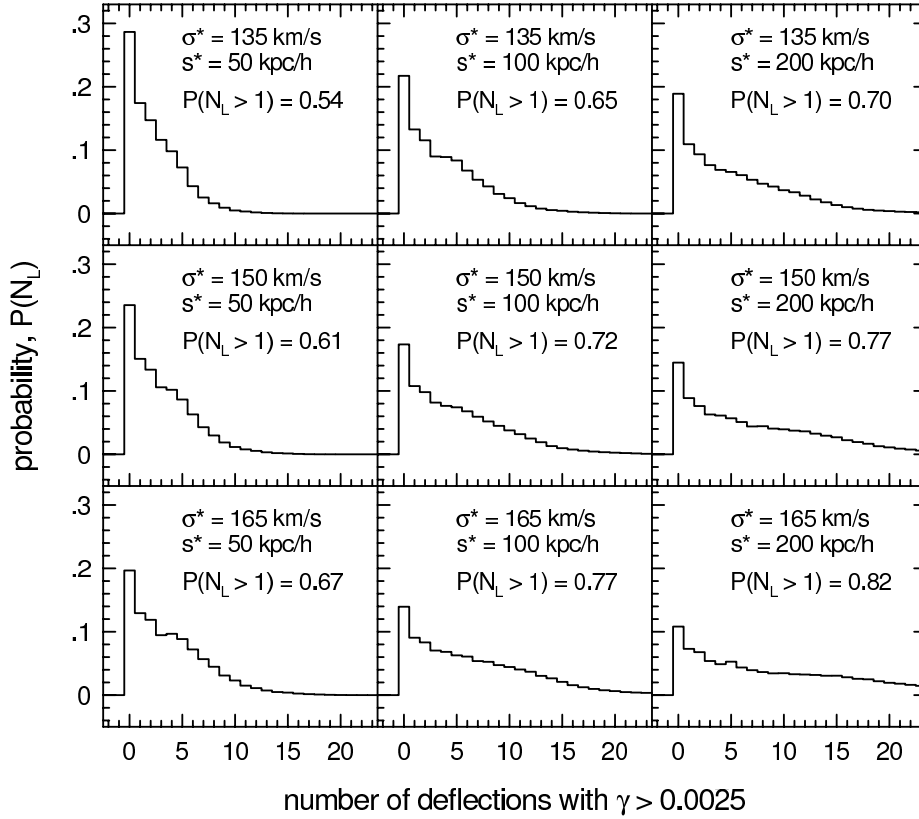
Fig. 5.— Probability, $P(N_L)$, that a source galaxy has been lensed by N_L foreground galaxies, where each individual lens induces a shear $\gamma > 0.0025$. For $N_L > 1$, multiple deflections with $\gamma > 0.0025$ have been experienced by the source. Here the sources have been distributed broadly in redshift space with a median redshift $z_s = 0.96$, and a flat Λ-dominated universe with $H_0 = 70$ km sec^{-1} Mpc^{-1}, $\Omega_{m0} = 0.3$ and $\Omega_{\Lambda 0} = 0.7$ has been adopted. Lens galaxies have a median redshift $z_l = 0.55$. Different panels correspond to different characteristic parameters (σ_v^*, s^*) adopted for the halos of L_B^* lens galaxies.
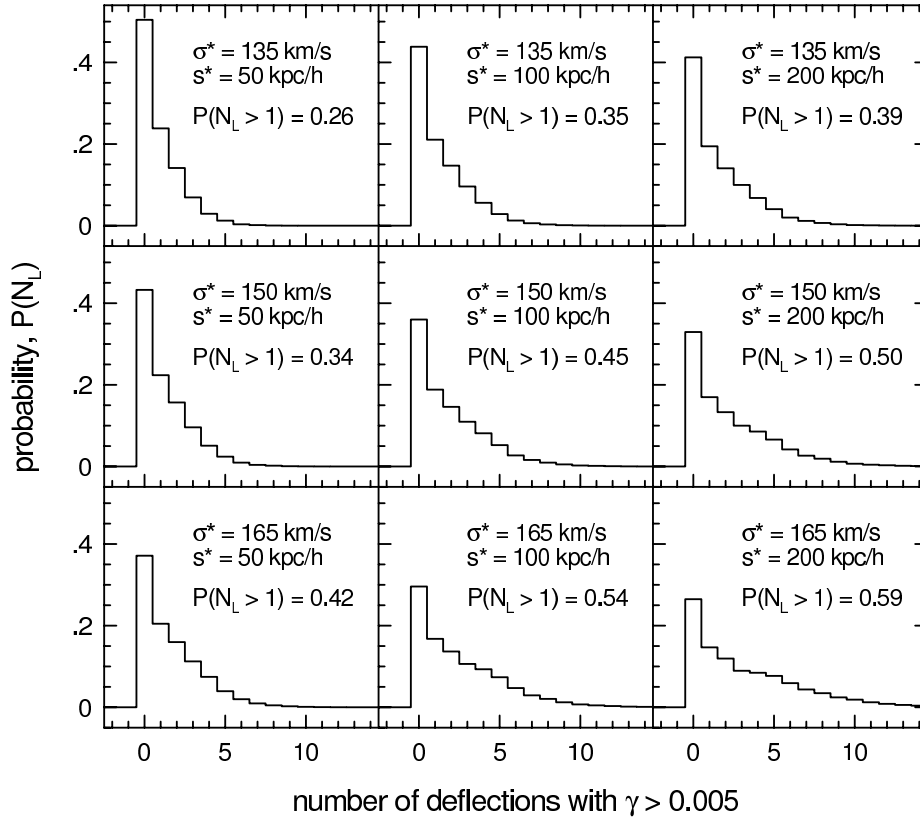
Fig. 6.— Same as Figure 5, except here the frequency of deflections with $\gamma > 0.005$ is shown. For $N_L > 1$, multiple deflections have been experienced by the source.
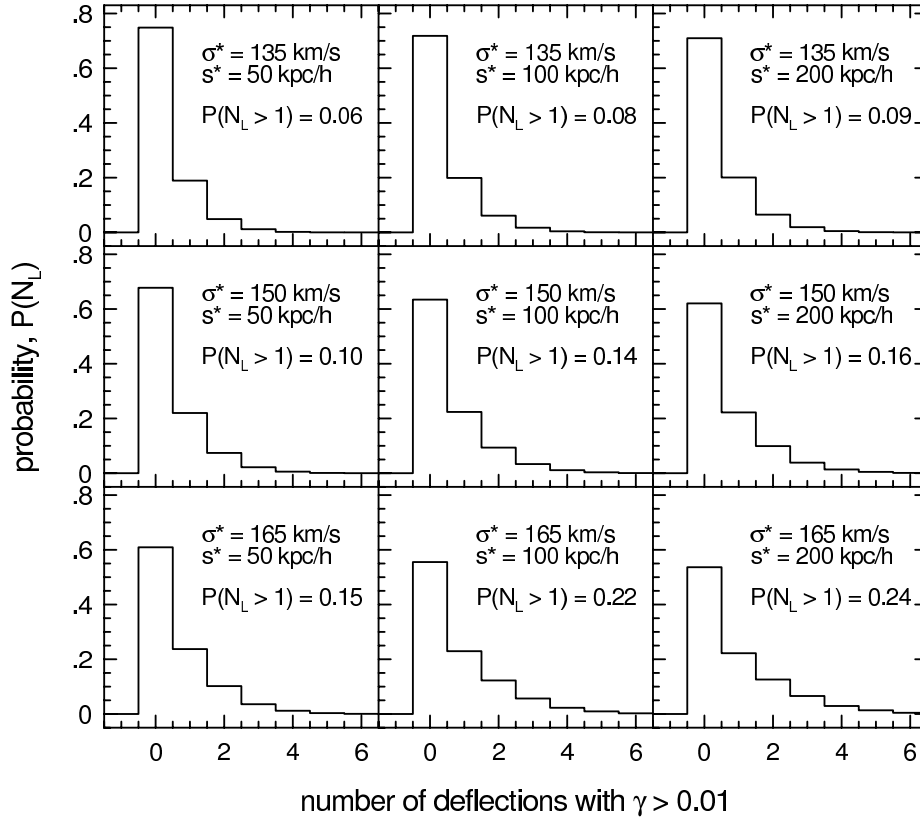
Fig. 7.— Same as Figure 5, except here the frequency of deflections with $\gamma > 0.01$ is shown. For $N_L > 1$, multiple deflections have been experienced by the source.

deflection calculation (γ_{max}). In particular, the following questions will be addressed:

- Is the closest weak lens (in projection on the sky) necessarily the most important weak lens?

- Is the net shear for a given source galaxy in the multiple-deflection calculation larger or smaller than the shear induced by the closest lens?

- Is the net shear for a given source galaxy in the multiple-deflection calculation larger or smaller than the shear resulting from the largest individual weak deflection?

- What effect does the inclusion of multiple deflections have on the mean tangential shear measured about the lens centers?

Throughout this section, source galaxies in the Monte Carlo simulations will be taken to have the broad redshift distribution used in Figure 1 (e.g., equation 6 above) and a flat Λ-dominated universe will be used.

The first question of this section is addressed in Figure 8. Here the probability distribution for the distance between the strongest individual weak lens, θ_{max}, and the closest weak lens, θ_{min}, is shown. The different panels correspond to different characteristic halo parameters that have been adopted for the halos of L_B^* galaxies (and appropriately scaled for all lenses according to equations 2 and 3 above). Figure 8 shows that, in general, the closest lens in projection on the sky is not the strongest individual weak lens. That is, of order 50% of the time the closest lens is not the "most important" weak lens. Figure 8 also shows the importance of performing the multiple-deflection calculation using sources that are contained within an area that is smaller than the area covered by the lenses, since the angular separation between the closest lens to a given source and the most important lens for that same source can reach scales of more than 2 arcminutes. In particular, $\sim 35\%$ of the strongest lenses have angular separations $\gtrsim 20$ arcsec from the sources and $\sim 10\%$ of the strongest lenses have angular separations $\gtrsim 60$ arcsec from the sources.

Figures 9 and 10 address the second and third questions of this section. That is, how does the net shear experienced by source galaxies in a full, multiple-deflection calculation compare to the shear due to only the closest lens (Figure 9) and to the shear due to the strongest individual weak lens (Figure 10)? Figure 9 shows that the net shear due to all foreground lenses is generally larger than the shear induced by the closest lens on the sky. The ratio of the shears, $\gamma_{net}/\gamma_{close}$, is weakly-dependent upon the specifics of the lens halo parameters. The probability that the net shear in the full multiple-deflection calculation exceeds the shear due to the single closest lens ranges from 78% (lens halos with small physical extents,
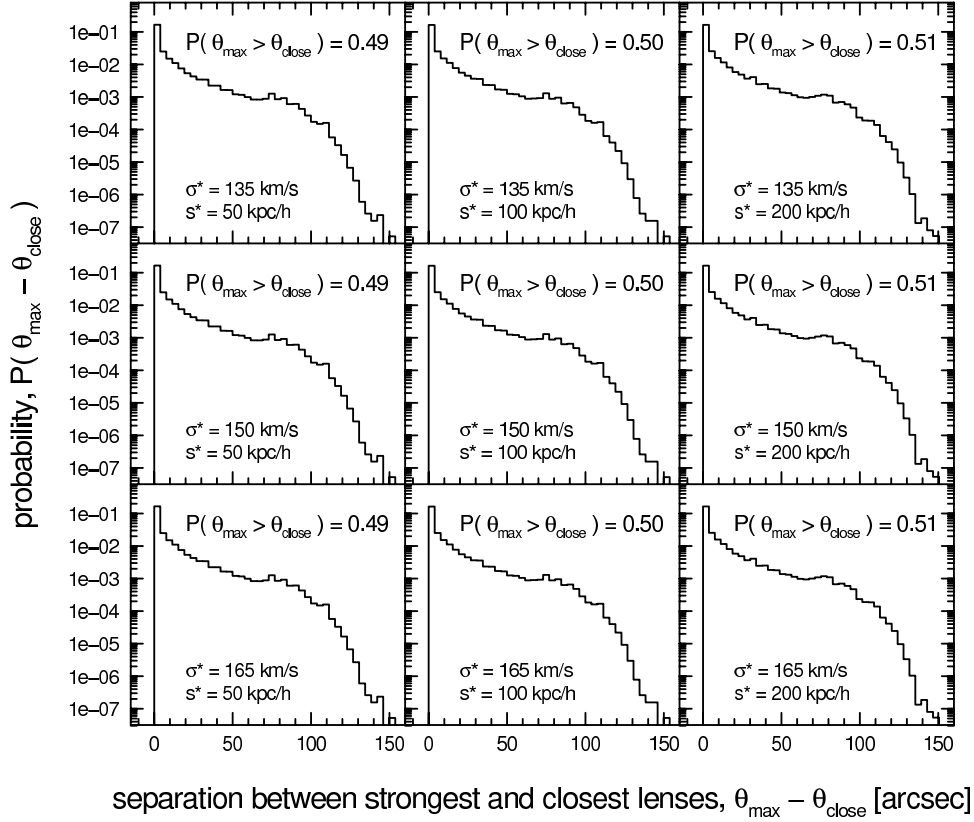
Fig. 8.— Probability distribution for the distance between the strongest individual weak lens for a given source, θ_{max}, and the closest individual weak lens for a given source, θ_{close}. The distance is zero when the closest lens is, in fact, the strongest lens for a given source. The probability that the strongest individual lens for a given source is not the closest lens is given in each panel, and is of order 50% in all cases. Different panels correspond to different characteristic halo parameters (σ_v^*, s^*) adopted for L_B^* lens galaxies.

$s^* = 50h^{-1}$ kpc) to 82% (lens halos with large physical extents, $s^* = 200h^{-1}$ kpc). Figure 10 shows that the net shear due to all foreground lenses is also generally larger than the shear induced by the strongest individual weak lens in the full, multiple-deflection calculation. As in Figure 9, the ratio of the shears, $\gamma_{\mathrm{net}}/\gamma_{\mathrm{max}}$, is weakly-dependent upon the specifics of the lens halo parameters. The probability that the net shear in the full multiple-deflection calculation exceeds the shear due to the single strongest weak lens ranges from 69% (lens halos with small physical extents, $s^* = 50h^{-1}$ kpc) to 76% (lens halos with large physical extents, $s^* = 200^{-1}$ kpc). Figures 9 and 10, then, show that for any given distant source galaxy, the net shear that its image experiences due to all foreground lenses exceeds the shear due solely to the closest lens, as well as the shear due solely to the strongest individual weak lens.

It may seem somewhat counter-intuitive that the net shear experienced by the images of distant source galaxies in the multiple-deflection calculations generally exceeds the shear due to a naive single-deflection calculation. That is, at first glance one might expect that multiple weak galaxy-galaxy lensing deflections should, on average, cancel each other. For a given source this would, indeed, be the case if all the foreground lenses were located at precisely the same angular separation from the source, had identical gravitational potentials, and had identical redshifts, z_l. Such an idealized situation is, of course, not the case in the real universe. That is, we cannot think in terms of a single lens plane for the galaxy-galaxy lensing problem, and to a certain extent the solution has to be understood numerically. This is due to the fact that there are a wide range of lens-source separations, the lenses have a wide range of gravitational potentials, and the lenses are distributed broadly in redshift. These, in combination, result in increased shear in the multiple-deflection calculation for galaxy-galaxy lensing, much as the non-uniformities in the mass distribution along the line of sight give rise to a net "cosmic shear" (see, e.g., reviews by Bartelmann & Schneider 2001; van Waerbeke & Mellier 2003; Refregier 2003; Munshi et al. 2008). That is, like galaxy-galaxy lensing, cosmic shear is inherently a multiple-deflection problem in which the deflections do not simply cancel. A detailed investigation of how the shear experienced by a given source galaxy is affected as one successively adds in more and more weak galaxy lenses will be presented in Howell & Brainerd (2010).

The last question of this section, the effect of multiple deflections on the mean tangential shear about the lens centers, is addressed in Figure 11. In Figures 9 and 10, we have computed quantities (net shear, shear due to the closest weak lens, and shear due to the strongest individual weak lens) that cannot, in practice, be measured in an observational data set. That is, without precise knowledge of the intrinsic shape of a source galaxy, the angular diameter distances of the source and all possible foreground lens galaxies, as well as the details of the gravitational potentials of all foreground lens galaxies, it is not possible to
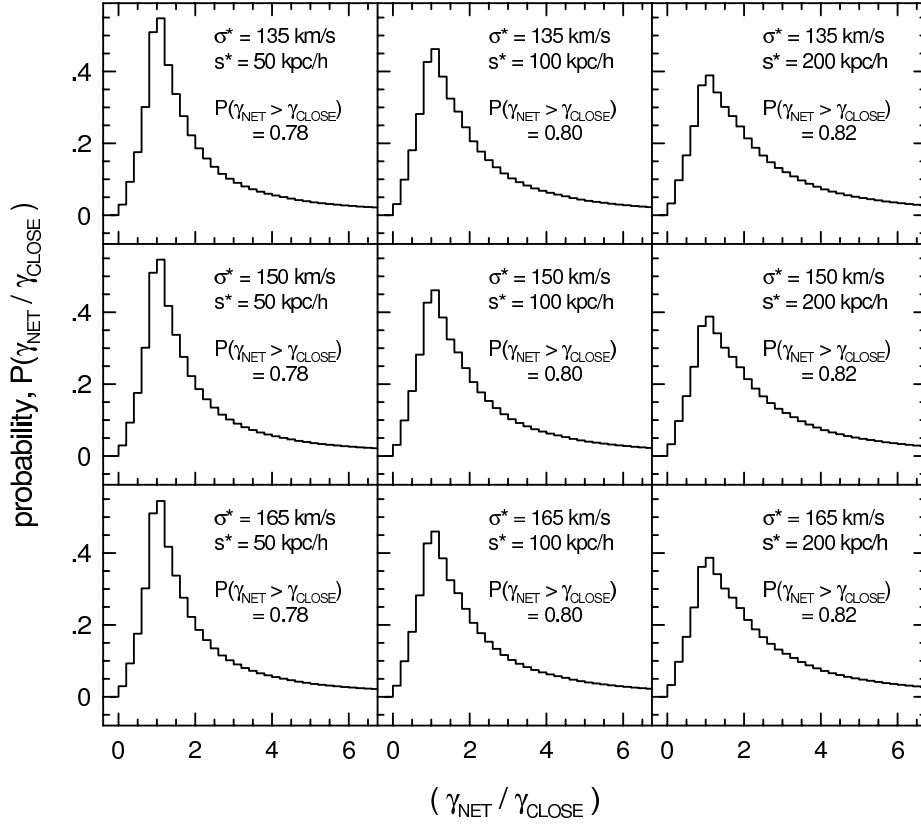
Fig. 9.— Probability distribution for the ratio of the net shear experienced by the images of source galaxies, γ_{net}, to the shear induced solely by the closest lens on the sky, γ_{close}. Different panels correspond to different characteristic halo parameters (σ_v^*, s^*) adopted for L_B^* lens galaxies. The probability that γ_{net} exceeds γ_{close} is listed in each panel.
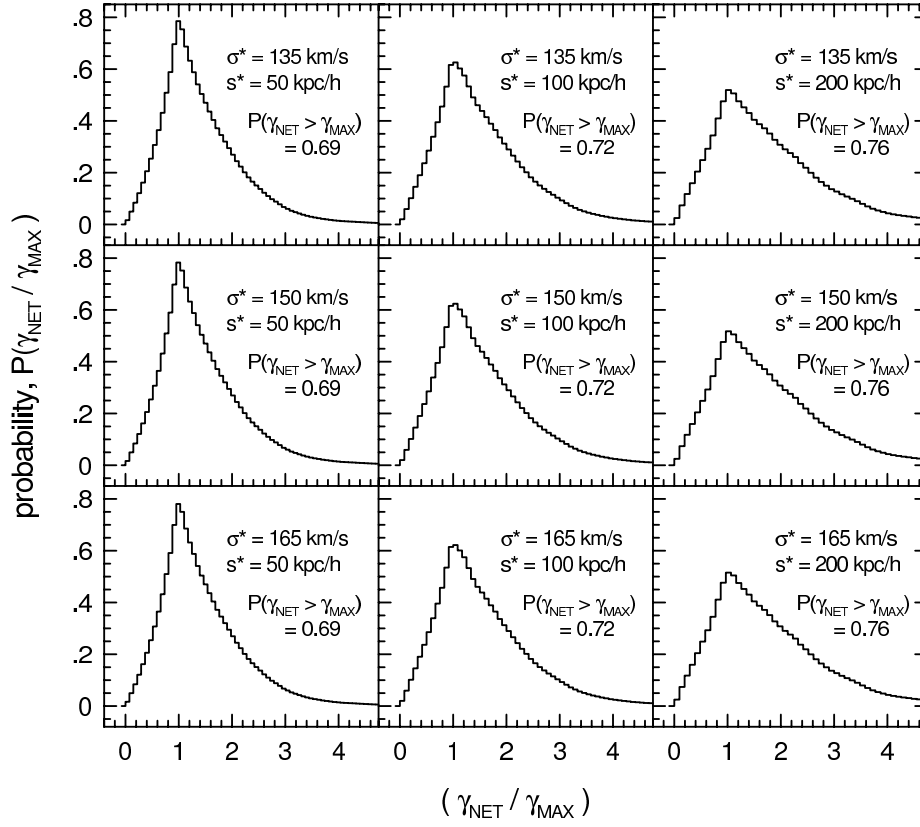
Fig. 10.— Same as Figure 9, except here the net shear, $\gamma_{\rm net}$, is compared to the shear induced by the strongest individual lenses in the multiple-deflection calculation, $\gamma_{\rm max}$.

deduce γ_{net}, γ_{close}, and γ_{max} for any one source galaxy. Indeed, galaxy-galaxy lensing yields such a small value of γ_{net} that it can only be detected via an ensemble average over the images of many source galaxies. Therefore, Figure 11 demonstrates the effect of multiple deflections on the *observable* galaxy-galaxy lensing signal: the mean tangential shear about the lens centers.

Shown in Figure 11 is the mean tangential shear, $\gamma_T(\theta)$, measured as a function of lens-source angular separation. Since the sources are restricted to a circle of radius 2.5 arcmin, while the lenses are restricted to a circle of radius 4.0 arcmin, it is not possible to compute $\gamma_T(\theta)$ around all of the lenses. Instead, $\gamma_T(\theta)$ is computed using only those lenses that are within a distance $r = (150 - \theta)$ arcsec of the center of the field. This allows the average to be computed in complete circular annuli, centered on each lens galaxy, and avoids edge effects. Solid squares in Figure 11 show $\gamma_T(\theta)$ for the full multiple-deflection calculations in which each source has been lensed by all foreground lenses. Open circles in Figure 11 show $\gamma_T(\theta)$ for single deflection calculations in which each source is lensed by only the closest lens on the sky. Shown in Figure 12 is the ratio of the mean tangential shears that are plotted in Figure 11. That is, Figure 12 shows the ratio of the mean tangential shear obtained from the full multiple-deflection calculations to that obtained from the single-deflection calculations.

From Figures 11 and 12, then, it is clear that on very small scales, galaxy-galaxy lensing reduces to a single-deflection problem. That is, on scales $\theta \sim 1$ arcsec, there is relatively little difference between the mean tangential shear obtained from the full, multiple-deflection calculations and the single deflection calculations. On scales of $\theta \gtrsim 2$ arcsec, however, the multiple deflection calculations yield a higher value of the mean tangential shear. The difference between $\gamma_T(\theta)$ from the multiple deflection calculations and $\gamma_T(\theta)$ from the single deflection calculations depends somewhat on the characteristic parameters adopted for the halos of L_B^* galaxies. On scales $\theta \sim 20$ arcsec, the multiple deflection calculation for the lowest mass halos (top left panel of Figure 12) yields a mean tangential shear that is a factor of ~ 1.4 larger than the mean tangential shear from the single deflection calculation. The multiple deflection calculation for the highest mass halos (bottom right panel of Figure 12) yields a mean tangential shear that is a factor of ~ 1.7 larger than the mean tangential shear from the single deflection calculation for $\theta \sim 20$ arcsec. It is also interesting to note that $\gamma_T(\theta)$ becomes roughly constant on scales $\theta \gtrsim 10$ arcsec. This is due to the fact that the mean angular separation between the lens galaxies is 10.7 arcseconds, which corresponds to a comoving distance of $48h^{-1}$ kpc at the median redshift of the lenses. That is, on angular scales comparable to and larger than the mean angular separation of the lenses, the halos of nearby lens galaxies are overlapping one another in projection on the sky. This is the primary reason that galaxy-galaxy lensing is not terribly sensitive to the radii of the halos of the lens galaxies.
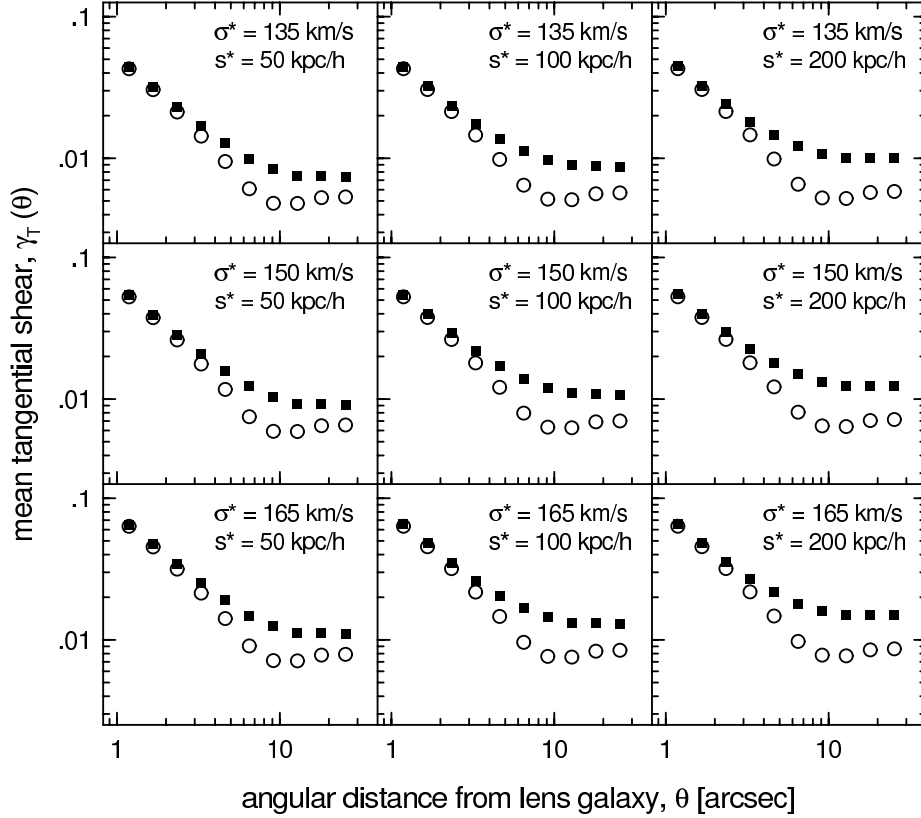
Fig. 11.— Mean tangential shear, $\gamma_T(\theta)$, computed in circular annuli of radius θ, centered on the lens galaxies. Different panels correspond to different characteristic parameters (σ_v^*, s^*) adopted for the halos of L_B^* lens galaxies. Solid squares: results of full multiple-deflection calculations in which source galaxies have been lensed by all foreground galaxies. Open circles: results of single-deflection calculations in which source galaxies are lensed only by the closest lens. The mean angular separation between the lenses is $\theta = 10.7''$.
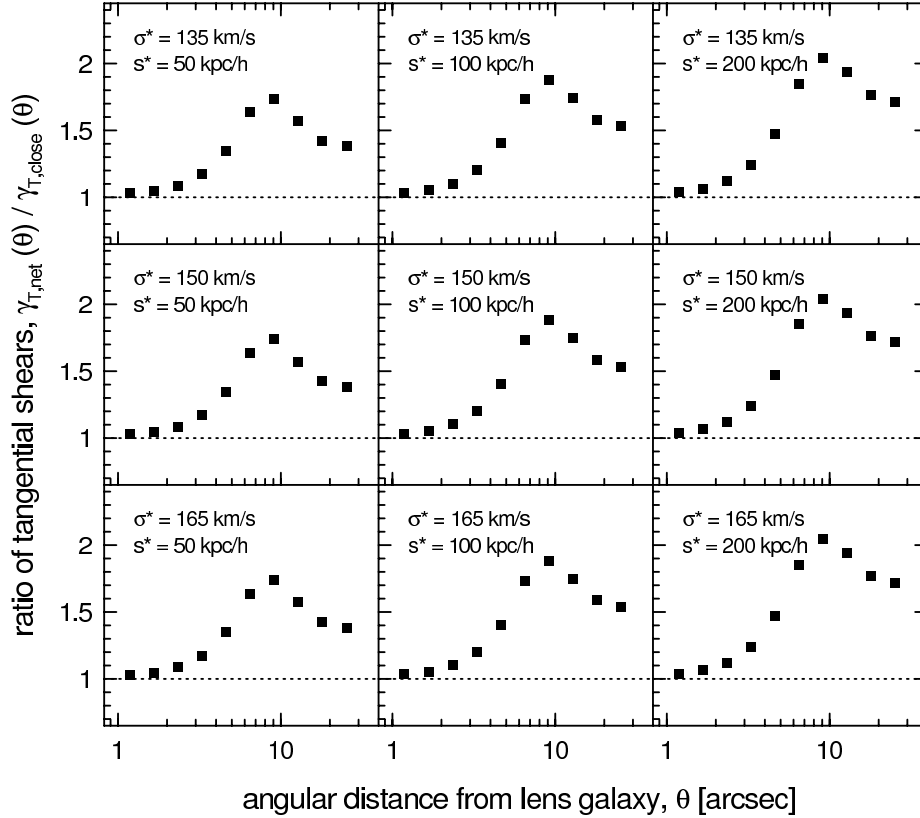
Fig. 12.— Ratio of the mean tangential shears shown in Figure 11. Different panels correspond to different characteristic parameters (σ_v^*, s^*), adopted for the halos of L_B^* lens galaxies. Dotted line indicates a value of unity. On scales of $\theta \gtrsim 2$ arcsec the mean tangential shear from the full multiple deflection calculations, $\gamma_{\mathrm{T,net}}(\theta)$, exceeds the mean tangential shear from the single-deflection calculations, $\gamma_{\mathrm{T,close}}(\theta)$.

It should be kept in mind that here we have only modeled the masses of the halos of individual galaxies. In particular, we have not included the fact that many of the larger, brighter galaxies are probably contained within group environments that have a substantial dark matter component over and above the dark matter halos of the individual galaxies. The circularly-averaged tangential shear (as we have computed here) is related to the surface mass density of a circular lens through

$$\gamma_T \Sigma_c = \overline{\Sigma}(< \theta) - \overline{\Sigma}(\theta) \equiv \Delta\Sigma \qquad (10)$$

(e.g., Miralda-Escudé 1991). In the case of completely isolated lens galaxies, $\Delta\Sigma$ above is the surface mass density of the dark matter halo of the lens galaxy. In the case of lenses that reside within groups and clusters, $\Delta\Sigma$ includes the mass due to the dark matter halos of the lens galaxies, as well as the mass of the larger dark matter halo that surrounds the group or cluster. In the case of bright, massive galaxies that reside in groups and clusters, the tangential shear shown in Figure 11 does not properly correlate with all of the mass that one would actually expect to contribute to the net shear in a observational data set. This is simply because we have neglected the additional mass associated with the environments in which those galaxies tend to reside.

Observations of galaxy-galaxy lensing have shown that the dependence of the tangential shear on projected distance from the lens is a function of the stellar mass and luminosity of the lens. In particular, the tangential shear measured around lens galaxies with low stellar masses and low luminosities is approximately constant at very large projected distances (e.g., Mandelbaum et al. 2006a, Figures 1 and 2), consistent with the results in Figure 11 above. However, the tangential shear measured around lens galaxies with high stellar masses and high luminosities declines monotonically at large projected distances (e.g., Mandelbaum et al. 2006a, Figures 1 and 2). This is due to the contribution of the overall mass within the relatively higher density environments in which the most massive, most luminous galaxies tend to reside. That is, in practice observed galaxy-galaxy lensing includes the effects of all individual galaxy lenses, as well as the effects of the mass within the local environment that surrounds the lenses. Here we have simply considered the effects of the individual halos of bright galaxies, and have not included environmental (e.g., group/cluster) contributions to the net shear.

The implications of Figures 11 and 12 are straightforward. If one wishes to use observations of $\gamma_T(\theta)$ to constrain the fundamental parameters associated with the halos of the lens galaxies (i.e., σ_v^* and s^* for the model adopted here), it is vital to use full, multiple-deflection Monte Carlo simulations for the parameter fitting. If simple, single-deflection calculations are used, the inferred halo masses will be systematically too large. That is, in order to reproduce an observed galaxy-galaxy lensing signal on angular scales greater than a few

arcseconds using a single-deflection calculation, one would need systematically larger halo masses than are required in the full multiple-deflection calculation.

5. Galaxy-Galaxy Lensing and Cosmic Shear

The galaxy-galaxy lensing contribution to cosmic shear is investigated in this section. Cosmic shear is often equated to weak lensing by the large-scale structure of the universe, but in practice cosmic shear is the result of photons from distant source galaxies being deflected by all mass along the line of sight. The mass along the line of sight includes large galaxy clusters, galaxy groups, and filaments, as well as objects with smaller masses such as individual galaxies. In the case of the galaxy-galaxy lensing, we are considering the specific contribution of the highly non-linear, large k contribution of the power spectrum of density fluctuations, $P(k)$, to the cosmic shear signal.

The source galaxies in the Monte Carlo simulations are assumed to have orientations that are intrinsically uncorrelated (i.e., each source is assigned an initially random position angle). Galaxy-galaxy lensing will, of course, slightly change both the ellipticity and the orientation of each source. In the presence of a number of high-mass lens galaxies that cause multiple weak deflections over large angular scales, the images of the source galaxies may acquire a net preferred orientation due to galaxy-galaxy lensing. This is the signature of cosmic shear, albeit in this case the shear is caused solely by the lens galaxies, not the entire large-scale structure of the universe.

To investigate the degree to which galaxy-galaxy lensing may contribute to the cosmic shear signal, the image correlation function

$$C_{\chi\chi}(\theta) = \left\langle \vec{\chi}_{f,i} \cdot \vec{\chi}_{f,j}^{*} \right\rangle_{\theta} \tag{11}$$

is computed. Here the mean is computed over all galaxy pairs i, j separated by an angle $\theta \pm d\theta/2$, $\vec{\chi}_{f,i}$ is the final shape parameter of source galaxy i, and $\vec{\chi}_{f,j}^{*}$ is the complex conjugate of the final shape parameter of galaxy j (see, e.g., Blandford et al. 1991). The correlation function measures the extent to which galaxy images "point" in the same direction on the sky. If $C_{\chi\chi}(\theta)$ is positive, the images of the galaxies are aligned with each other. If $C_{\chi\chi}(\theta)$ is zero, the images of the galaxies are randomly oriented. If $C_{\chi\chi}(\theta)$ is negative, the images of the galaxies tend to be oriented perpendicular to each other (i.e., they are anti-aligned).

Shown in Figure 13 is the image correlation function for the source galaxies, where the galaxies have again been broadly distributed in redshift space and a flat Λ-dominated universe has been adopted. Solid squares show the results for the full, multiple-deflection calculations and open circles show the results for the single-deflection calculations in which

the sources have been lensed by only the closest lenses. From Figure 13, then, it is clear that for angular separations $\theta \gtrsim 5$ arcsec, the single-deflection calculations yield essentially no contribution of galaxy-galaxy lensing to the cosmic shear. That is, if multiple deflections were not important in galaxy-galaxy lensing, one would expect that on scales greater than 5 arcsec, galaxies alone would not contribute to cosmic shear. Hence, cosmic shear on scales greater than 5 arcsec would be expected to be largely independent of the gravitational potentials of the halos of field galaxies. However, the full, multiple-deflection calculations in Figure 13 show that galaxy-galaxy lensing can, indeed, induce substantial correlations in the source images on scales greater than 5 arcsec. Furthermore, the degree of lensing-induced image alignment is strongly affected by the characteristic parameters that are adopted for the halos of L_B^* lenses.

In addition to the image correlation function, the top hat shear variance

$$\langle \gamma^2 \rangle = \frac{2}{\pi \theta^2} \int_0^\infty \frac{dk}{k} \, P_\kappa(k) \left[J_1(k\theta) \right]^2 \tag{12}$$

is common measure of cosmic shear. Here P_κ is the power spectrum of the projected mass density of the universe, J_1 is a Bessel function of the first kind, and θ is the radius of the circular aperture over which the mean is computed. In an observational data set, the function is computed as

$$\langle \gamma^2 \rangle = \frac{1}{N(N-1)} \sum_{i \neq j} \vec{\gamma}_i \cdot \vec{\gamma}_j^*, \tag{13}$$

for all galaxies within a circular aperture of radius θ on the sky. Solid squares in Figure 14 show the shear top hat variance due to galaxy-galaxy lensing alone, obtained from full, multiple-deflection calculations. Again, sources have been broadly distributed in redshift and a flat Λ-dominated universe is adopted. Also shown for comparison (crosses connected by dotted line) are the measured values of $\langle \gamma^2 \rangle$ obtained by Fu et al. (2008) for galaxies in the CFHT Legacy Survey with a median redshift $z_m = 0.83$. Although this is somewhat lower than the median redshift of the source galaxies in the Monte Carlo simulations, it is sufficiently similar that it is reasonable to compare the observational and theoretical results directly.

From Figure 14, the small-scale contribution of galaxy-galaxy lensing to $\langle \gamma^2 \rangle$ depends quite strongly on the parameters adopted for the halos of L_B^* galaxies, and scales roughly with the relative masses of the halos. For example, the lowest mass L_B^* lenses (top left panel) have masses that are a factor of 2.5 smaller than those of the fiducial halo with $\sigma_v^* = 150$ km sec^{-1} and $s^* = 100h^{-1}$ kpc (middle panel). Similarly, the highest mass L_B^* lenses (bottom right panel) have masses that are a factor of 2.4 larger than those of the fiducial halo. At $\theta = 1$ arcmin, $\langle \gamma^2 \rangle$ for the lowest mass lenses is a factor of 3 smaller than
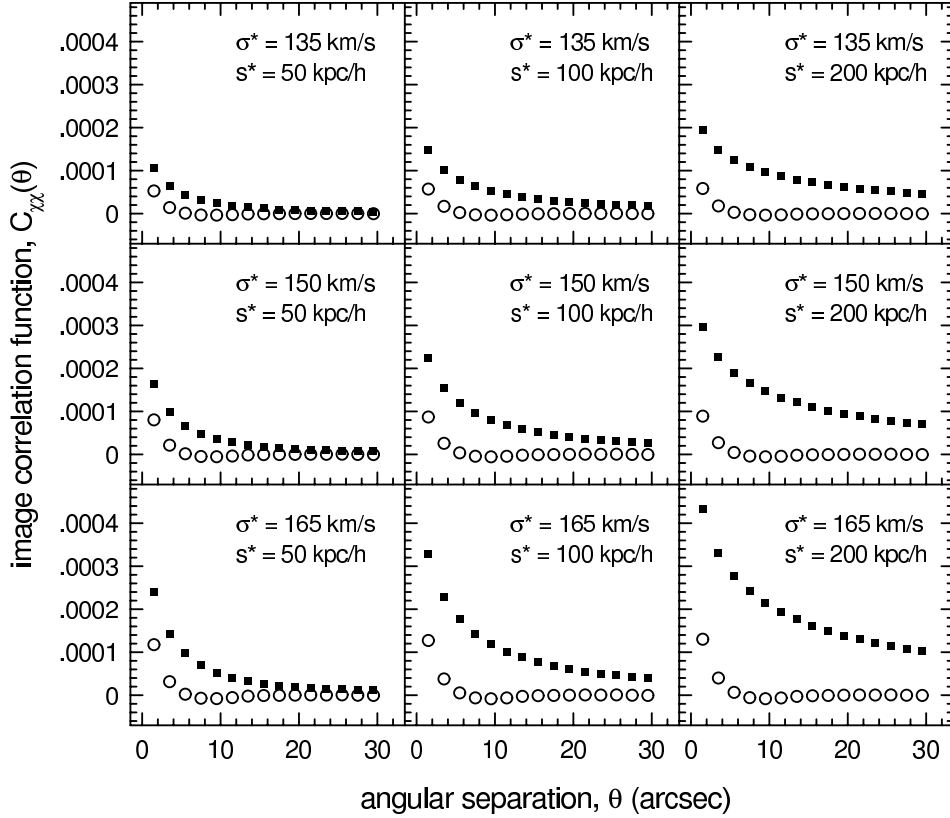
Fig. 13.— Image correlation function, $C_{\chi\chi}(\theta)$, due to galaxy-galaxy lensing alone. Different panels correspond to different characteristic parameters (σ_v^*, s^*) adopted for the halos of L_B^* galaxies. Solid squares: results of full multiple-deflection calculations in which source galaxies have been lensed by all foreground galaxies. Open circles: results of single-deflection calculations in which source galaxies are lensed only by the closest lens.

it is for the fiducial halo, and $\langle \gamma^2 \rangle$ for the highest mass lenses is a factor of 3.5 larger than it is for the fiducial halo.

Comparing the squares in Figure 14 (simulation results) to the crosses (observational results), it is clear that, depending upon how deep the potential wells of L_B^* galaxies are, galaxy-galaxy lensing alone may contribute a substantial amount to cosmic shear. In the case of the lowest mass L_B^* halos, galaxy-galaxy lensing alone would be expected to contribute only $\sim 5.5\%$ of the value of $\langle \gamma^2 \rangle$ measured by Fu et al. (2008) for an aperture of radius $\theta = 1$ arcmin. In the case of the fiducial L_B^* halos, the contribution of galaxy-galaxy lensing alone increases to $\sim 16\%$ for $\theta = 1$ arcmin, while for the highest mass L_B^* halos $\sim 58\%$ of the signal seen by Fu et al. (2008) at $\theta = 1$ arcmin would be due to galaxy-galaxy lensing alone. If one were to extrapolate the Fu et al. (2008) results to scales $\theta < 1$ arcmin, the results shown in the bottom right panel of Figure 14 suggest that the halos of L_B^* galaxies are probably not as large adopted in this particular panel. That is, a simple extrapolation of the Fu et al. (2008) result to $\theta < 1$ arcmin leads to an expectation of much less observed cosmic shear than is predicted by galaxy-galaxy lensing by our highest mass lenses.

Because of the relatively small area of the sky that is covered by the sources in the Monte Carlo simulations, it is not possible to compute $\langle \gamma^2 \rangle$ on large angular scales. However, the rms value, $\langle \gamma^2 \rangle^{1/2}$, decreases linearly with θ and it is, therefore, straightforward to extrapolate the results from Figure 14 to an angular scale at which the contribution of galaxy-galaxy lensing to cosmic shear vanishes. From this extrapolation, then, the contribution of galaxy-galaxy lensing to cosmic shear vanishes at $\theta = 5.0$ arcmin for the lowest mass halos, $\theta = 5.2$ arcmin for the fiducial model, and $\theta = 5.4$ arcmin for the highest mass halos. Therefore, although the contribution of galaxy-galaxy lensing to cosmic shear on small angular scales is very sensitive to the details of the gravitational potentials of galaxies, cosmic shear on scales $\theta \gtrsim 5$ arcmin should not be affected by galaxy-galaxy lensing to any significant degree.

6. Cosmic Variance

The shear field in the Monte Carlo simulations comes from a set of lenses that are contained within an area of 50 sq. arcmin. on the sky and, therefore, one might be concerned that the results shown above could be compromised by cosmic variance. Here some of the results above are recomputed using subdivisions of the data in order to explore potential small field effects. To do this, we use the fiducial model in which the halos of L_B^* galaxies have velocity dispersions of $\sigma_v^* = 150$ km sec^{-1} and characteristic radii of $s^* = 100h^{-1}$ kpc, we take the sources to be broadly distributed in redshift as above, and we use a flat Λ-dominated cosmology.
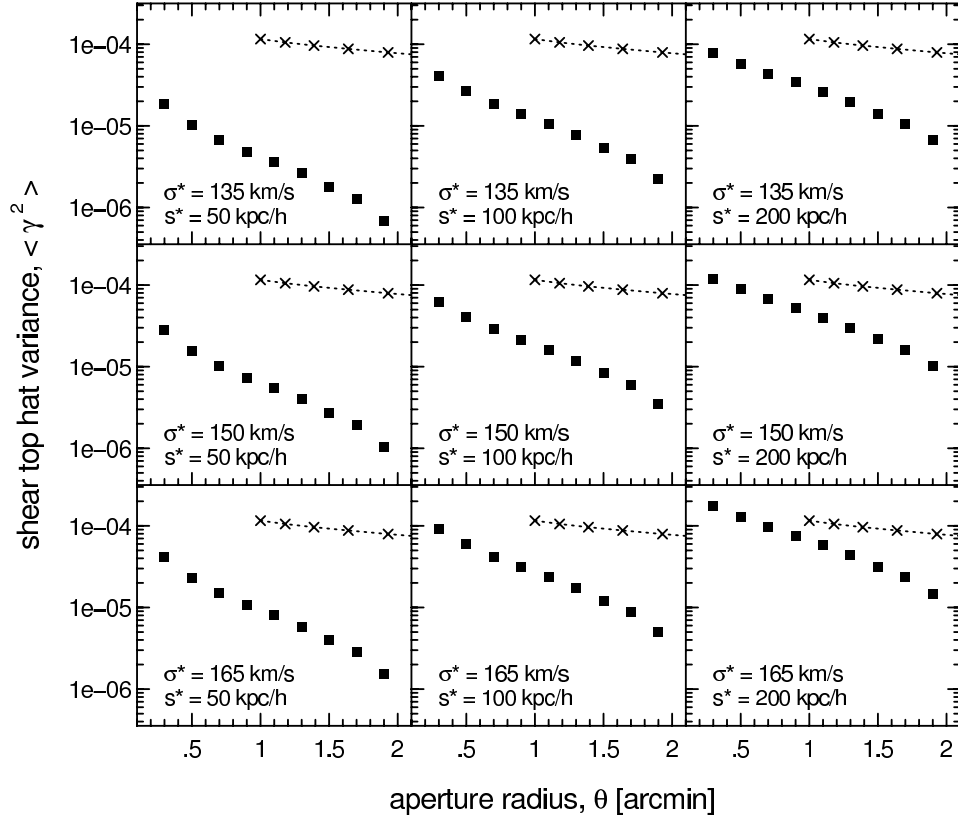
Fig. 14.— Solid squares: top hat shear variance, $\langle\gamma^2\rangle$, due to galaxy-galaxy lensing alone, obtained from the full multiple-deflection calculations. Different panels correspond to different characteristic parameters $(\sigma_v^*, \ s^*)$ adopted for the halos of L_B^* galaxies. Shown for comparison (crosses connected by dotted line) are the results from Fu et al. (2008) for the top hat shear variance obtained from the CFHT Legacy Survey using sources with median redshift $z_s = 0.83$.

Shown in Figure 15 is a comparison of the frequency of multiple deflections that give rise to individual shear values of $\gamma > 0.005$ (top panels), the mean tangential shear about the lens centers, $\gamma_T(\theta)$ (middle panels), and the image correlation function, $C_{\chi\chi}(\theta)$ (bottom panels) using different subdivisions of the data. The left hand panels show a comparison of results obtained from data in the northern half of the field and results obtained from data in the southern half of the filed. The right hand panels show results obtained from data in the eastern half of the field and results obtained from data in the western half of the field. While there are some differences that result when the size of the field is reduced by a factor of two, the differences are small and suggest that the results obtained from the full field should not suffer dramatically from effects of cosmic variance.

7.   Conclusions

The frequency and effects of multiple weak lensing deflections in galaxy-galaxy lensing have been investigated using Monte Carlo simulations. The lenses in the simulations are modeled using observed galaxies with magnitudes $R \leq 23$, contained within a circle of radius of 4 arcminutes, centered on the HDF-N. The lenses have known redshifts and known rest-frame B-band luminosities. By adopting a simple halo mass model it is possible to determine the relative strengths of each of the lenses using scaling relations.

The Monte Carlo simulations reveal a number of expected results: (i) the frequency of multiple deflections depends upon the minimum value of the shear (i.e., the lower is the minimum value, the more likely it is that multiple deflections will be experienced by a given source), (ii) the frequency of multiple deflections depends upon the source redshift (i.e., the higher is the source redshift, the more likely it is that will experience multiple deflections) and (iii) the higher are the masses of the lenses, the more likely it is that multiple deflections will occur. For a deep galaxy-galaxy lensing data set in which the sources have a median redshift $z_s \sim 1$ and the lenses have a median redshift $z_l \sim 0.6$, the probability that a given source galaxy will have experienced more than one weak lens that induces a "typical" shear of $\gamma = 0.005$ ranges from 26% to 59%, depending upon the masses adopted for the lenses.

The Monte Carlo simulations also reveal a number of results that may seem counter-intuitive at first glance: (i) of order 50% of the time, the closest lens in projection on the sky is not the most important weak lens for a given source, (ii) for a given source, the net shear due to all foreground lenses generally exceeds the shear due to the strongest individual weak lens, and (iii) multiple deflections give rise to a larger tangential shear around the lens galaxies than a simple, single-deflection calculation in which the closest lens is assumed to be the only lens. This emphasizes the importance of using full, multiple-deflection calculations when
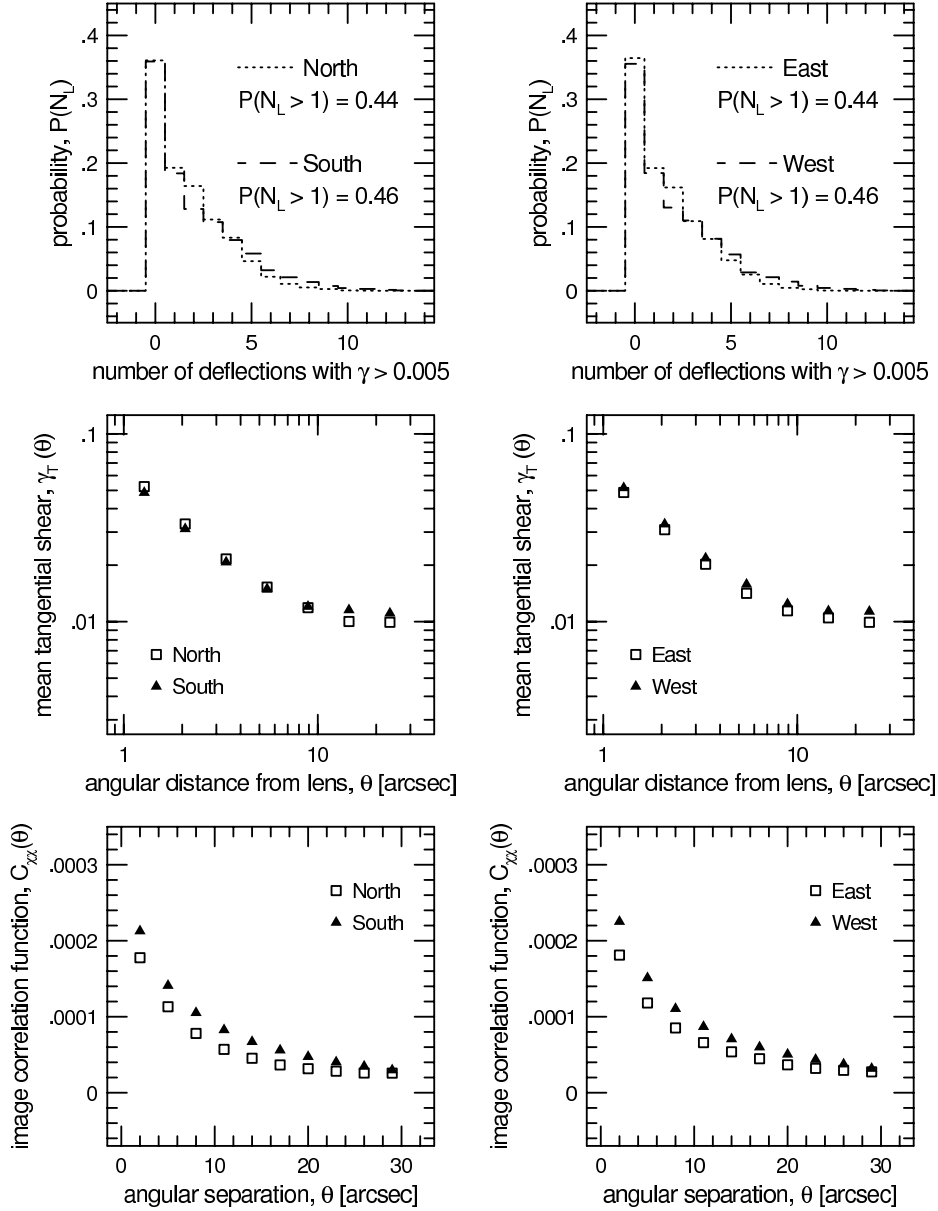
Fig. 15.— Comparison of the frequency of multiple weak deflections (top), the mean tangential shear (middle), and the image correlation function (bottom) for different subdivisions of the field. Left: comparison of results from the northern half of the field to results from the southern half of the field. Right: comparison of results from the eastern half of the field to results from the western half of the field. Here the sources have been broadly distributed in redshift with $z_{\mathrm{med}} = 0.96$. The fiducial halo model with $\sigma_v^* = 150$ km sec^{-1} and $s^* = 100h^{-1}$ kpc, and a flat Λ-dominated cosmology have also been adopted.

using observations of galaxy-galaxy lensing to constrain the parameters of the dark matter halos of the lens galaxies. If multiple deflections are not incorporated into the calculation, this will result in halo masses that are systematically too large.

Lastly, the Monte Carlo simulations reveal that galaxy-galaxy lensing alone can give rise to a cosmic shear signal on small angular scales. This is unsurprising because cosmic shear occurs when photons from distant galaxies are deflected by all mass along the line of sight. In the case of galaxy-galaxy lensing, it is the very large k end of the power spectrum of density fluctuations that contributes to the cosmic shear by inducing correlated image shapes for the distant galaxies. On scales $\theta \sim 1$ arcmin, the degree to which galaxy-galaxy lensing contributes to cosmic shear is quite sensitive to the masses of the lens galaxies. Changing the mass of the halo of a fiducial L_B^* galaxy by a factor of ~ 2.5 changes the contribution to the top hat shear variance, $\langle \gamma^2 \rangle$, by a factor of ~ 3. Comparing the theoretical values of $\langle \gamma^2 \rangle$ at $\theta = 1$ arcmin to the value observed by Fu et al. (2008) for sources with a similar redshift distribution, galaxy-galaxy lensing alone could account for as little as $\sim 5\%$ or as much as $\sim 58\%$ of the observed value, depending upon the halo mass for L_B^* galaxies.

While the small-scale contribution of galaxy-galaxy lensing to cosmic shear is quite sensitive to the masses of the lenses, the scale at which galaxy-galaxy lensing becomes unimportant to cosmic shear is relatively independent of the lens masses. If the results for the galaxy-galaxy lensing contribution to cosmic shear are extrapolated to large scales, the contribution of galaxy-galaxy lensing to cosmic shear should vanish for scales $\theta \gtrsim 5$ arcmin, largely independent of the lens masses.

Acknowledgments

REFERENCES

Bartelmann, M. & Schneider, P. 2001, Phys. Rep., 340, 297

Blandford, R. & Narayan, R. 1986, ApJ, 310, 568

Blandford, R. D., Saust, A.-B., Brainerd, T. G. & Villumsen, J. V. 1991, MNRAS, 251, 600

Brainerd, T. G., Blandford, R. D. & Smail, I. 1996, ApJ, 466, 623 (BBS)

Cohen, J. G., Cowie, L. L., Hogg, D. W., Songaila, A., Blandford, R., Hu, E. M. & Shopbell, P. 1996, ApJ, 471, L5

Cohen, J. G., Hogg, D. W., Blandford, R., Cowie, L. L., Hu, E., Songaila, A., Shopbell, P., & Richberg, K. 2000, ApJ, 538, 29

Cohen, J. G. 2001, AJ, 121, 2895

Cooray, A. & Hu, W. 2001, ApJ, 574, 19

dell'Antonio, I. P. & Tyson, J. A. 1996, ApJ, 473, L17

Fischer, P. et al. 2000, AJ, 120, 1198

Fu, L, Semboloni, E., Hoekstra, H., Kilbinger, M., van Waerbeke, L., Tereno, I., Mellier, Y., Heymans, C., Coupon, J., Benabed, K., Benjamin, J., Bertin, E., Dore, O., Hudson, M. J., Ilbert, O., Maoli, R., Marmo, C., McCracken, H. J. & Menard, B. 2008, AA, 479, 9

Guzik, J. & Seljak, U. 2002, MNRAS, 335, 311

Heymans, C., Bell, E. F., Rix, H.-W., Barden, M., Borch, A., Caldwell, J. A. R., McIntosh, D. H., Meisenheimer, K., Peng, C. Y., Wolf, C., Beckwith, S. V. W., Haussler, B., Jahnke, K., Jogee, S., Sanchez, S. F., Somerville, R. & Wisotzki, L. 2006, MNRAS, 371, L60

Hilbert, S., Hartlap, J., White, S. D. M. & Schneider, P. 2009, AA, 499, 31

Hoekstra, H., Yee, H. K. C. & Gladders, M. D. 2004, ApJ, 606, 67

Hoekstra, H., Hsieh, B. C., Yee, H. K. C., Lin, H. & Gladders, M. D. 2005, ApJ, 653, 73

Hogg, D. W., Pahre, M. A., Adelberger, K. L., Blandford, R., Cohen, J. G., Gautier, T. N., Jarrett, T., Neugebauer, G. & Steidel, C. C. 2000, ApJS, 127, 1

Howell, P. & Brainerd, T. G. 2010, in preparation

Hudson, M. J., Gwyn, S. D. J, Dahle, H. & Kaiser, N. 1998, ApJ, 503, 531

Kleinheinrich, M., Schneider, P., Rix, H.-W., Erben, T., Wolf, C., Schirmer, M., Meisen-
    heimer, K., Borch, A., Dye, S., Kovacs, Z. & Wisotzki, L. 2006, AA, 455, 441

LeFevre, O., Hudon, D., Lilly, S. J., Crampton, D., Hammer, F. & Tresse, L. 1996, ApJ,
    461, 534

LeFevre, O. et al. 2004, AA, 428, 1043

Limousin, M., Kneib, J.-P., Bardeau, S., Natarajan, P., Czoske, O., Smail, I., Ebling, H. &
    Smith, G. P. 2007, AA, 461, 881

Lowenthal, J. D., et al. 1997 ApJ, 481, 673

Mandelbaum, R., Seljak, U., Kauffmann, G., Hirata, C. M. & Brinkmann, J. 2006a, MNRAS,
    368, 715

Mandelbaum, R., Hirata, C. M., Broderick, T., Seljak, U. & Brinkmann, J. 2006b, MNRAS,
    370, 1008

Miralda-Escudé 1991, ApJ, 370, 1

Munshi, D., Valageas, P., van Waerbeke, L. & Heavens, A. 2008, Phys. Rep., 462, 67

Natarajan, P., Kneib, J.-P., Smail, I., Treu, T., Ellis, R., Moran, S., Limousin, M. & Czoske,
    O. 2009, ApJ, 693, 970

Parker, L. C., Hoekstra, H., Hudson, M. J., van Waerbeke, L. & Mellier, Y. 2007, ApJ, 669,
    21

Phillips, A. C., Guzman, R., Gallego, J., Koo, D. C., Lowenthal, J. D., Vogt, N. P., Faber,
    S. M. & Illingworth, G. D. 1997, ApJ, 489, 543

Refregier, A. 2003, ARAA, 41, 645

Schneider, P., Ehlers, J. & Falco, E. E. 1992, Gravitational Lenses (Berlin: Springer)

Sheldon, E., Johnston, D. E., Frieman, J. A., Scranton, R., McKay, T. A., Connolly, A. J.,
    Budavari, T., Zehavi, I., Bahcall, N. A., Brinkmann, J. & Fukugita, M. 2004, AJ,
    127, 2544

Smail, I., Hogg, D. W., Yan, L. & Cohen, J. G. 1995, ApJ, 449, L105

Steidel, C. C., Giavalisco, M., Dickinson, M. & Adelberger, K. L. 1996, AJ, 112, 352

Tian, L., Hoekstra, H. & Zhao, H. 2009, MNRAS, 393, 885

van Waerbeke, L. & Mellier, Y. 2003 (arXive:0305089)

Williams, R. E., Blacker, B., Dickinson, M., Dixson, W. V. D., Ferguson, H. C., Fruchter, A. S., Giavalisco, M., Gilliand, R. L., Heyer, I., Katsanis, R., Levay, Z., Lucas, R. A., McElroy, D. B., Petro, L., Postman, M., Adorf, H.-M. & Hook, R. 1996, AJ, 112, 1335